The chamber design of the L-shaped oscillating water column using artificial neural network

C.-C. Lin, Y.-C. Chow, and D. T. Nguyen

Abstract—**Among the various wave energy converters available, the oscillating water column (OWC) shows several advantages in implementation and maintenance. In dealing with the survivability issues, incorporating OWCs into reinforced concrete constructions, like breakwaters, is more cost-effective and can endure the effects of seawater impact and erosion. This paper focuses on optimizing the chamber design of a novel OWC type, the L-shaped OWC, by establishing a general design procedure to achieve higher power-capturing efficiency. The performance of the OWC is influenced significantly by the OWC's geometry under a specified wave condition. It is found that the dimension of the air chamber and water duct is critical in determining OWC's performance. We develop the chamber design procedure based on the artificial neural network approach by establishing a collection of two-dimensional RANS simulations as the training database. In the end, the performance of the optimal design is compared with the design of a previous paper. The result shows that the capture factor of the present optimized chamber geometry of the L-shaped OWC is 60% more than a former design.**

Keywords—**Artificial neural network, chamber design, L-shaped, Oscillating water column.**

I. Introduction

Several operational instances of Oscillating Water Column (OWC) plants combined with breakwaters have been documented. One example is the Sakata Harbor wave power plant in Japan, which incorporated a Wells turbine into its breakwater [1]. Similarly, the harbor of Civitavecchia in Italy features the U-OWC [2] and the Mutriku Wave Power Plant in the port of Mutriku, Spain [3].

Given Taiwan's moderate wave resources, implementing OWC technology offers several advantages. Firstly, OWCs can be seamlessly integrated into existing onshore structures, specifically reinforced concrete breakwaters. This approach significantly reduces installation and maintenance costs, while the concrete structure provides superior resistance against seawater impact and erosion. The survival capability of OWC structures is of utmost importance in Taiwan due to the region's exposure to extreme weather conditions during the typhoon season, making it highly resilient in harsh environments.

The OWC has been comprehensively studied among various types of Wave Energy Converters (WEC) [4]. Since the 1970s, OWCs have been the subject of theoretical analysis [5-7], numerical simulation [8-10], and experimentation [11-13]. Chamber geometry is considered the most crucial factor affecting the performance of OWCs. Rezanejad et al. [14] analyzed the effect of a stepped bottom on the efficiency of nearshore OWCs based on two-dimensional linear water wave theory. Bouali and Larbi [15] used ANSYS to investigate the geometry and dimensions of the OWC to obtain the maximum available power in progressive wave characteristics. Kim et al. [16] applied potential flow simulation to describe the hydrodynamic response of an inclined OWC. López et al. [17] used OpenFOAM simulation to compare with experimental results, suggesting the optimized geometry of L-shaped OWC (abbreviated as L-OWC) and U-shaped OWC (abbreviated as U-OWC) under the wave conditions at the Port of Vigo, Spain. The results showed that the L-OWC outperforms the U-OWC in terms of performance. The L-OWC geometry, with a shallow entrance, a high horizontal chamber duct, and a vertical duct, delivers a maximum capture-width ratio of 71.6%. Tsai et al. [18] investigated the performance of a Modified Breakwater-

This work was supported by National Academy of Marine Research under grant no. NAMR-110-014.

Prof. C. C. Lin is with the department of mechanical and mechatronic engineering and Center for Ocean Energy System, National Taiwan Ocean University, Keelung 202301, Taiwan, ROC (e-mail: cclin@email.ntou.edu.tw).

Prof. Y. C. Chow is with the department of systems engineering and naval architecture and Center for Ocean Energy System, National Taiwan Ocean University, Keelung 202301, Taiwan, ROC (e-mail: ycchow@email.ntou.edu.tw).

D. T. Nguyen is Ph.D. candidate with the department of systems engineering and naval architecture, National Taiwan Ocean University, Keelung 202301, Taiwan, ROC (e-mail: 10551013@email.ntou.edu.tw).

Digital Object Identifier: https://doi.org/10.36688/ewtec-2023-555

Integrated OWC WEC under Taiwan's wave climate using Flow-3D simulation and experimental investigation. Their full-scale numerical simulation showed that the hydrodynamic efficiency could reach 83% when the air orifice area ratio is 0.7%.

Geometric optimization methodologies based on machine learning or artificial neural networks have emerged in recent years. For example, Lin et al. [19] established an artificial neural network (ANN) model to study the performance of cylindrical oscillating wave surge converters (OWSCs) and obtained a geometric shape with a very high capture factor (CF). Liu et al. [20] applied ANN to predict the CFs of OWSCs and used a genetic algorithm to search for the optimal result.

The L-OWC and U-OWC have their pros and cons. In terms of performance, the L-OWC generally has a much higher energy conversion efficiency, i.e., a higher CF or capture width ratio (CWR), compared to the U-OWC, while the U-OWC has a broadband performance, i.e., its CF is more uniformly distributed across the wave spectrum. In terms of cost, the L-OWC is usually larger in size than the U-OWC, resulting in higher material and installation costs for the L-OWC. The choice between the two models depends on developers' careful calculations and considerations to determine the "best" selection. This paper will focus on the L-OWC due to its high power capture performance. The optimal geometric design is critical for implementing Taiwan's OWC wave power system. This paper establishes the optimal chamber design procedure through two-dimensional numerical simulation and the ANN approach. The optimal design will be compared with the previous design by López et al. [17].

II. DESIGN AND ANALYSIS METHODOLOGY

A. OWC Design Theory

The free surface in an OWC's plenum chamber can be modeled to be a massless piston, oscillating up and down harmonically with an incident plane wave of amplitude A_i and angular ω in the y axis such that its position $Y(t)$ can be expressed as

$$Y(t) = \mathrm{Re}\left[A_Y e^{-i\omega t} \right] \tag{1}$$

where A_Y denotes the complex amplitude of $Y(t)$ and $y = 0$ is the still-water level (SWL). Therefore, the equation of motion for the oscillator (i.e., the piston-like free surface) in the frequency domain can be expressed as

$$F_E = \left[-\omega^2 \mu_A - i\omega\left(\nu_f + \nu_{PTO}\right) + \rho g S \right] A_Y \tag{2}$$

where F_E denotes the complex amplitude of the wave exciting force; μ_A the added mass due to the oscillation of the water column; ν_f and ν_{PTO} the damping coefficients due to the linearized fluid effects of wave radiation and viscosity, and the PTO (Power Take-off), respectively; ρ the density of the seawater; g the acceleration of gravity; S the area of the free surface of the water column in the OWC's plenum chamber. After some algebraic manipulations, (2) can be transformed into

$$\left|A_Y\right|^2 = \frac{\left|F_E\right|^2}{\mu_A^2\left(\omega^2 - \omega_o^2\right)^2 + \omega^2\left(\nu_f + \nu_{PTO}\right)^2} \tag{3}$$

where

$$\omega_o = \sqrt{\frac{\rho g S}{\mu_A}} \tag{4}$$

The term ω_o can be regarded as the natural frequency of the OWC due to gravity and the added mass of the water column. In a wave period $T = 2\pi/\omega$, the average power taken off by the PTO can be calculated with

$$P = \frac{1}{T}\int_0^T \nu_{PTO}\left(\dot{Y}\right)^2 dt = \frac{\omega^2 \nu_{PTO}}{2}\left|A_Y\right|^2 \tag{5}$$

The capture factor, CF, is defined and can be calculated with

$$CF \equiv \frac{P}{P_i} = \frac{P}{\frac{1}{2}\rho g \left|A_i\right|^2 C_g B} = \left(\frac{\omega^2 \nu_{PTO}}{\rho g \left|A_i\right|^2 C_g B} \right)\left|A_Y\right|^2 \tag{6}$$

where P_i denotes the incident wave power contained within B, the OWC's width facing the wave; C_g the incident wave's group velocity.

Combining (3) and (6) with some algebra, CF can be written as

$$CF = \left(\frac{\left|F_E\right|^2}{4\rho g \left|A_i\right|^2 \nu_f C_g B} \right)\left\{ \frac{4\left(\nu_f \cdot \nu_{PTO}\right)}{\omega^2 \mu_A^2\left[1 - \left(\frac{\omega_o}{\omega}\right)^2\right]^2 + \left(\nu_f + \nu_{PTO}\right)^2} \right\} \tag{7}$$

It can be shown that when

$$\begin{cases} \omega_o = \sqrt{\dfrac{\rho g S}{\mu_A}} = \omega \\ \nu_{PTO} = \nu_f \end{cases} \tag{8}$$

The second bracket on the right-hand-side of (7) is maximized to be 1, i.e., the OWC attains its resonance with the maximized CF as

$$CF_{@res} = \frac{|F_E|^2}{4\rho g |A_i|^2 \nu_f C_g B} \tag{9}$$

The OWC theory, as described above, enables us to deduce helpful design guidelines because it integrates components of mechanism affecting OWCs' performances and clarify the relations among them. For example, it is evident from (9) that $CF_{@res}$ increases as ν_f decreases, leading to a design guideline for reducing the wave radiation (the major part of the linearized fluid effects) from the OWC as much as possible. One can also use this theory for the regression and curve fitting of the data obtained from any experiment or numerical simulation of OWC to estimate critical hydrodynamic coefficients associated with a specific OWC geometry, i.e., $|F_E|$, ν_f and μ_A. It can be expected that this theory and associated analyses will illuminate how both high-peak power output and broad-band-responsive performance can be achieved in the OWC design.

B. *Design procedure*

The OWC design procedure consists of two primary steps. The first step involves ensuring the reliability of the simulation software, while the second step focuses on optimizing the geometric design of the OWC chamber. This study employs the commercial software Flow-3D to simulate the hydrodynamic behavior of the L-OWC and identify the most suitable chamber geometry. However, it is crucial to validate the software's reliability before proceeding with the design process. This validation is achieved in the first step by conducting wave tank tests on a model of the OWC. The data gathered from these tests is then used to verify the accuracy of the numerical simulation results. In the second step, a comprehensive L-OWC performance database is established, encompassing various chamber dimensions for a specific wave condition. Subsequently, an artificial neural network is trained and employed to predict the optimal chamber geometry.

C. *Experimental Validation*

To validate the simulation results, an experiment was carried out using a 1/20th scale model. The experiments took place in the wave tank of the Hydraulic Laboratory, situated at the Department of Harbor & River Engineering of National Taiwan Ocean University. The layout of the experimental setup for this model experiment is depicted in Fig. 1. A high-speed camera was utilized to capture time-series images of the water levels within the OWC chamber. An image processing and analysis procedure was developed to determine the positions of the moving water levels.

1) *Wave tank and incident wave conditions*

The experimental wave tank has dimensions of 28 m in length, 2.0 m in width, and 0.8 m in height. Figure 2 illustrates the wavemaker used in the experiment, which was designed and manufactured by Edinburgh Design Ltd. This wavemaker can generate regular and irregular waves based on the user's instructions. Wave gauges were positioned at the longitudinal middle plane of the wave tank.

The experiment encompassed four incident wave conditions, each consisting of two wave periods (1.9 sec and 2.35 sec) and two wave heights (0.05 m and 0.075 m). These values were derived from wave data collected from the coastal waters of northeast Taiwan, and they were scaled down to a 1/20th ratio. Table 1 provides a visual representation of these wave conditions. Throughout the experiment, the water depth in the wave flume was maintained at 0.5 m.

TABLE 1 INCIDENT WAVE CONDITIONS OF SIMULATION AND EXPERIMENTS.

Parameters	scaled dimension (1/20th)
Wave height H	0.05 m, 0.075 m
Wave period T	1.9 s, 2.35 s
Water depth h	0.5 m
Wave number kh	0.679, 0.823

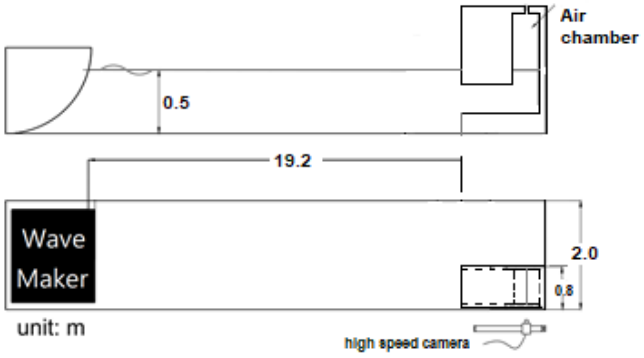

Fig. 1. Schematic of the L-OWC model experimental setup

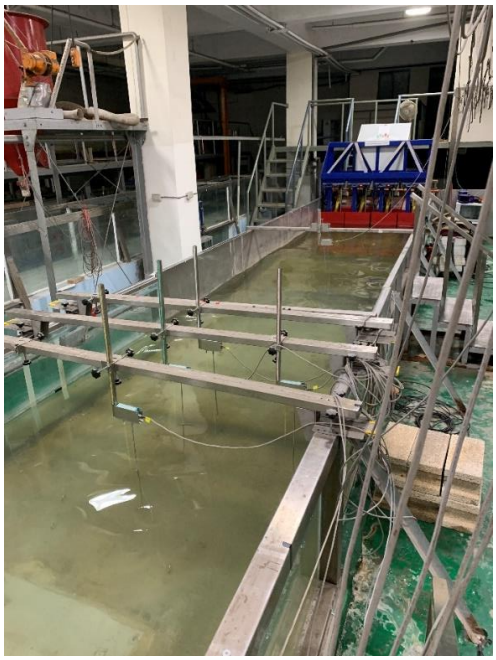

Fig. 2. Displacement piston wavemaker and wave tank

2) The experimental model specifications

As previously mentioned, experiments were conducted to validate the accuracy of the numerical results. Consequently, all the parameters of the L-OWC experimental model align with its numerical setup. Table 2 provides specific details regarding the parameters of the 1/20th scale L-OWC experimental model, including two different air chamber slot widths: w = 0.005 m and 0.01 m, representing varying PTO damping. Combining these four sets of wave conditions with the two air chamber slot widths results in a total of eight experimental conditions. The transverse width of the L-OWC model in the wave tank was selected as 0.8 m (as shown in Fig. 1) to ensure both the structural strength and rigidity of the model and the quasi-2D flow characteristics of the water in the conduit and air chamber. These characteristics were verified through observations of the nearly flat and horizontal free surface during water column oscillations.

TABLE 2 GEOMETRIC PARAMETERS OF 1/20TH SCALED BASELINE MODEL OF L-OWC.

Geometric parameters of the baseline model	Value (m)
Chamber width *a* (X-dir)	0.233
Length of duct *b*	0.585
Depth of duct *c*	0.13
Height of duct inlet *d*	0.16
Height of chamber *f*	0.695
Height of foundation *e*	0.21
Water depth *h*	0.5
OWC breadth (Y-dir)	0.3
Slot width *w*	0.005, 0.01

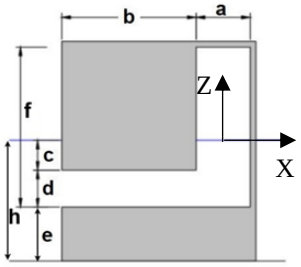

3) Numerical simulation

Figure 3 depicts the computational domain and mesh settings, incorporating the L-OWC model. The meshing strategy utilizes two blocks: the wave area block (block 1) and the L-OWC block (block 2). To address the two-fluids modeling problem, RANS simulations are conducted using the FLOW-3D software package. The k-ω model is employed for these simulations. Fluid 1 represents water at 20 degrees, while fluid 2 represents air at 25 degrees. Given the small-scale nature of the model, air compressibility can be disregarded [21]. Consequently, both water and air are treated as incompressible flows throughout this series of simulations.

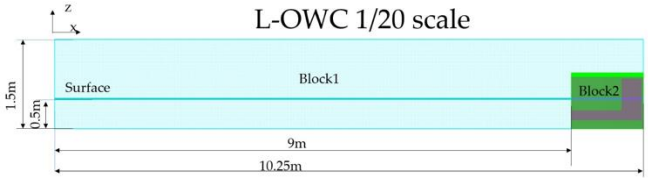

Fig. 3. The schematic of the computation domain and mesh setting

The Response Amplitude Operator (RAO) is used to evaluate the response of the different OWC designs under different incident wave conditions, according to López et al. [17]. The RAOs include RAO_c and RAO_P, where RAO_c represents the response amplitude operator of the water level difference inside the chamber, and RAO_P represents the response amplitude operator of pressure difference.

The definitions are expressed as follows

$$RAO_c = \frac{H_c}{H_i} \tag{12}$$

$$RAO_p = \frac{\Delta p}{\rho_w g H_i} \tag{13}$$

where H_i is the incident wave height, H_c is the average water level difference of the water column inside the chamber, Δp is the air pressure difference, ρ_w is the density of water, and g is the acceleration of gravity.

Since the measurement of the air pressure difference requires fairly accurate measuring instruments, this paper will only use RAOc to compare results between numerical simulation and the experiment.

The capture factor CF, which is the ratio between captured power and incident wave power, can be rewritten as equation (14):

$$CF = \frac{P_{air}}{P_i} = \frac{P_{air}}{\frac{1}{8} B \rho_w g H_i^2 C_g} \tag{14}$$

$$P_{air} = \frac{1}{T}\int_0^T P_E dt = \frac{1}{T}\int_0^T \Delta p \cdot Q dt \tag{15}$$

$$P_E = \Delta p \cdot Q \tag{16}$$

Among which, P_{air} represents the average power of air to PTO (such as turbine), P_E is the instantaneous power of the air, and P_i is the incident wave power per unit.

4) High-speed imaging

As shown in Fig. 4, the Phantom v310 CMOS high-speed camera with a maximum resolution of 1280 x 800 pixels and an acquisition rate as high as 3200 fps was used to capture the water level inside the L-OWC chamber model (shown in Fig. 5) through the transparent tempered glass on the sidewall of the wave flume.

The wave gauges and the high-speed camera were installed together to simultaneously capture the time series of the change of incident wave height and the water level inside the OWC chamber.

Fig. 4. Phantom v310 CMOS high-speed camera.

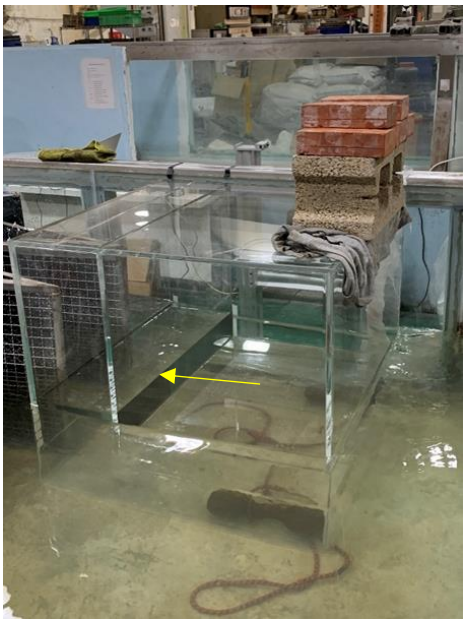

Fig. 5. The water level line inside the L-OWC chamber

5) Image processing and analysis procedures

The initial image capturing the time series of the water-air interface inside the OWC chamber is imported into the MATLAB program for image processing tasks such as denoising, contrast enhancement, and filtering.

By applying Canny edge detection, the water level becomes clearly distinguishable. Consequently, each point on the water level line can be accurately located. These points are then averaged to determine the average position of the water level line.

Subsequently, the average distance between the upper and lower boundaries of the water level can be calculated using H_c in (12).

6) Comparison between experimental and numerical simulation results

Table 3 presents a comparison between the experimental and numerical simulation results of the L-OWC. Each experiment value represents the average value obtained after three repetitions.

One notable observation is that the RAOc (Response Amplitude Operator in heave motion) values obtained from the numerical simulations are generally higher than those from the experiments. The differences range from approximately 3% to 7%, with the minimum difference compared to the experiment being -0.25%. These disparities could be attributed to various factors that are not observable in the experiment, such as friction loss on the wall surface. In situations where the response amplitude is significant, the water surface inside the air chamber can be drawn towards the horizontal channel, leading to errors in the results.

On the whole, the experimental results align reasonably well with the numerical results, considering the average difference values. Hence, the current software used for the

L-OWC numerical simulation can be considered acceptable in terms of reliability.

TABLE 3. RAO_c OF EXPERIMENTAL AND NUMERICAL SIMULATION

Slot width w Wave conditions (T, H)	RAO_c Exp.	RAO_c Sim.	Difference %
w=0.005m T=1.9s / H=0.05m	2.42	2.53	4.39
w=0.005m T=2.35s / H=0.05m	4.30	4.61	7.23
w=0.005m T=1.9s / H=0.075m	2.30	2.43	5.58
w=0.005m T=2.35s / H=0.075m	3.75	3.87	3.22
w=0.01m T=1.9s / H=0.05m	2.58	2.70	4.54
w= 0.01m T=2.35s / H=0.05m	4.81	4.80	-0.25

III. OPTIMIZATION OF OWC CHAMBER

The relationship between the model's geometric parameters and the OWC's capture factor is highly nonlinear and typically cannot be expressed explicitly. However, it is possible to address the multi-dimensional mapping challenge using a two-layer feed-forward network with sigmoid hidden neurons by utilizing consistent data sets. With the artificial neural network algorithm, Matlab's neural network fitting tool can be employed to discover this functional relationship when provided with input-output data. These data sets are used to train the network and determine the optimal functional relationship.

Matlab's neural network fitting tool (Nftool) mainly uses three algorithms: 1 Bayesian Regulation (BR), 2. Levenberg Marquardt (LM) and 3. Scaled Conjugate Gradient (SCG) to train the static fitting of a standard two-layer feedforward neural network. Generally, the Bayesian Regulation algorithm can obtain relatively good prediction results when dealing with a small number of samples but relatively more noise. The number of training data sets here is only 32, so we adopted the Bayesian Regulation algorithm.

The training data is established from the results of numerical simulation using Flow-3D. Various sets of design parameters of L-OWC's chamber are fed into the Flow-3D to obtain the results, i.e., the corresponding capture factor. The data sets are randomly divided into 70% for training, 5% for validation, and 25% for testing. The ANN performance is evaluated using mean square error (MSE) and regression analysis. The training data set updates the weight and bias according to the error. The test data set provides a way to analyze ANN performance during and after training, so the test data does not affect training. When the generalization process stops improving (note: generalization is the ability of a machine-learning algorithm to adapt to fresh samples), training stops automatically.

The more training data provided, the higher the prediction accuracy. Therefore, we need to provide sufficient data to improve the prediction accuracy of the ANN. In Table 2, we have selected five parameters: the width of the air chamber a, the length of duct b, the depth of the duct inlet c, the height of duct d, and the ratio of slot width to the chamber width w/a. The parameters a, b, c, d are the actual design parameters, whereas w/a is regarded as the PTO's damping value. We set the low-level and high-level values of the five parameters as shown in Table 4. To establish the training data set, we chose two values in each parameter range; one is the parameter value 20% above the low-level value, and the other is 20% below the high-level value in the corresponding range of each design parameter. In total, there are $2\times2\times2\times2\times2 = 32$ combinations of parameter sets for the simulation of the L-OWC. All simulations were performed under the regular wave condition with a wave period of 1.9s and a wave height of 0.075m.

We adopted Bayesian Regulation algorithm for the training process. The ANN is implemented by one hidden layer with ten cells. Figure 6 shows the regression performance of the training process, and Fig. 7 shows the convergence behavior of the training process. The regression performance is considered to be a pretty good fit where Training R is 1 and Test R is 0.99494. The convergence behavior of the training is regarded as excellent as the mean squared error achieved 2.5055e-14 at epoch 154.

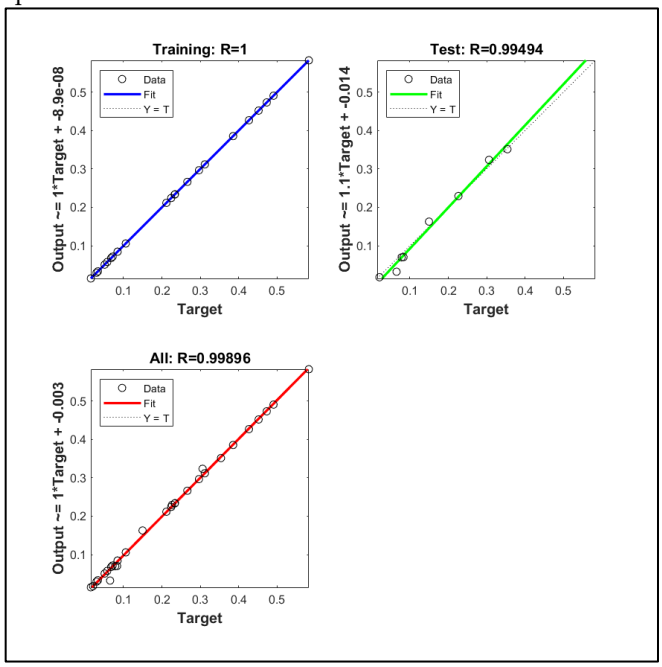

Fig. 6 Regression performance of the ANN model for LOWC

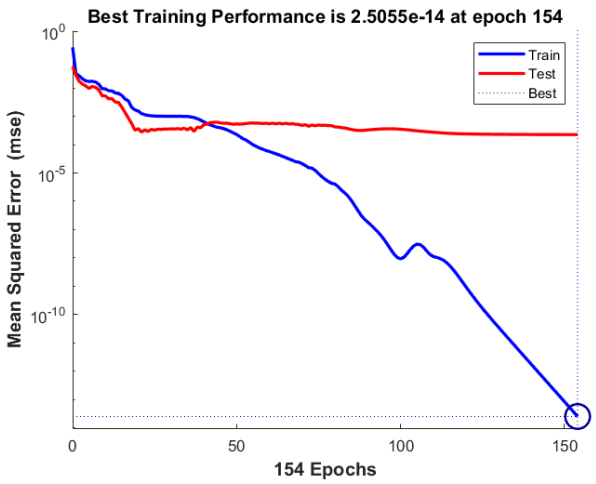

Fig. 7 The convergence behavior of an ANN training process

TABLE 4 THE LOWER BOUNDS, UPPER BOUNDS, INCREMENTS, AND THE NUMBER OF SAMPLED POINTS FOR ANN TRAINING AND PREDICTION (UNIT IN M).

Design parameter	Low-level value	High-level value	Increment of sampled points for prediction	Number of sampled points for prediction
a	0.192	0.384	0.002	97
b	0.487	0.976	0.003	164
c	0.108	0.217	0.005	22
d	0.133	0.267	0.01	14
w/a	0.014	0.03	0.002	9

Total combinations of predicted points: 44,096,976

Once the ANN training/learning process is finished, the function generated by Matlab's fitting tool can be utilized to predict the capture factor for any sampled points within the range of the design parameters (*a, b, c, d,* and *w/a*). For the L-OWC, the current prediction focuses on a wave period of 1.9 seconds and a wave height of 0.075 meters, which correspond to T = 8.5 seconds and H = 1.5 meters in real sea conditions.

Table 5 specifies the parameter sets of the sampled points for prediction, each within the designated range of the respective parameter. The total number of parameter combinations for prediction is 97 × 164 × 22 × 14 × 9 = 44,096,976.

Subsequently, the maximum capture factor value can be determined by evaluating all the predicted CFs. In the current case, completing all the CF predictions and searching for the maximum CF value required approximately 1118 seconds.

Finally, the optimal design parameters are fed back into Flow-3D to obtain the simulation results for comparison with the predicted values.

IV. RESULTS AND DISCUSSION

A. Result of optimization

Table 5 presents the geometric parameters resulting from the ANN optimization process for the L-OWC chamber. It includes the predicted maximum capture factor (CF_{ANN}) obtained through ANN and the CF value (CFSIM) obtained from Flow-3D simulation using identical design parameters. The results demonstrate that CF_{ANN} is only 9% smaller than CF_{SIM}, indicating a strong regression result.

It is important to highlight that the CF_{ANN} function is derived from the regression analysis of the input data set during the training process. Discrepancies may arise if the training data set does not fully capture the behavior of the physical system. In the current case, the training data's largest CF is approximately 0.6, as shown in the training window of Figure 6. This suggests that the predicted CF values exceeding 0.6 may not be as accurate, considering that the output performance is determined by the input parameters.

However, this issue can be addressed by providing more input data sets, for example, 3^5 (81) data sets, for the current case. By expanding the training data set, the accuracy of the predicted CF values can be improved. In conclusion, the ANN optimization process is viable and valuable in identifying the optimal design parameters, but it benefits from a comprehensive and representative input data set.

TABLE 5 THE OPTIMIZATION RESULT OF L-OWC @T = 1.9 S

Design parameter	Optimal parameter value	CF_{ANN}	CF_{F3D}
Chamber width *a*	0.192		
Length of duct *b*	0.976		
Depth of duct *c*	0.108	0.8	0.88
Height of duct inlet *d*	0.263		
w/a	0.014		

B. Performance evaluation of the optimal chamber design

Figure 8 shows the CF comparison between the present optimized L-OWC (#3 @ T = 8.5s) and the results of Ref. [17] (#1 @ T = 8s, #2 @ T = 10s). The capture factor in the present optimized case is 23.6% higher than case #2, and 60% higher than case #1. We may conclude that the optimized L-OWC significantly improves power capture performance.

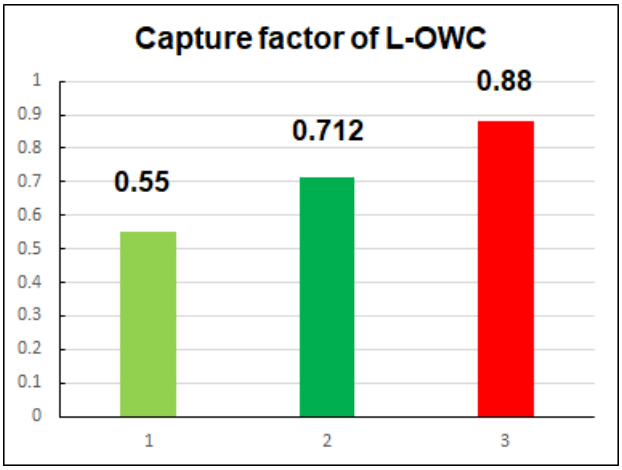

Fig. 8 The comparison of capture factors of the present optimized L-OWC (#3 @T = 8.5s) and the results of Ref. [17] (#1 @T = 8s, #2 @T = 10s)

The optimized design parameter values obtained in this research indicate that the values for chamber width *a* and the depth of the duct *c* tend to be at the lower end of their specified bounds. On the other hand, the values for the duct length *b* and the height of the duct inlet *d* tend to be at the higher end of their specified bounds. The above observations suggest that extending the parameter values beyond the current specified bounds can potentially achieve higher performance.

From the optimized design parameters, we can conclude that the chamber width *a* and the depth of duct *c* should be kept smaller, whereas the duct length *b* and the height of the duct inlet *d* should be kept larger.

V. CONCLUSIONS

The paper demonstrates the optimization process for the chamber design of L-OWC wave energy converters. The utilization of the ANN algorithm enables the establishment of an efficient functional relationship between the input design parameters and the capture factor, allowing for accurate prediction of the capture factor. Through this optimization process, the final chamber design exhibits improved power-capturing efficiency compared to the design presented in a previous research study [17].

In summary, the main conclusions of the paper are as follows:

1. The chamber geometry of the L-OWC plays a crucial role in determining its power capture performance. The optimized design of the L-OWC in this research achieves a capture factor of 0.88 with wave periods of 8.5 seconds, which is 60% higher than the CF (=0.55) obtained by the best design in the previous paper [17] under similar wave conditions.
2. It is recommended to keep the chamber width *a* and the depth of the duct *c* relatively smaller, while maintaining larger values for the duct length *b* and the height of the duct inlet *d*.
3. The design optimization utilizing the ANN approach is proven feasible and highly efficient in predicting the capture factor (CF), despite the predicted values being slightly smaller than the simulated values. However, it is important to note that the prediction accuracy can be further improved by incorporating additional input data sets into the training process.

REFERENCES

[1] M. Suzuki, C. Arakawa, and S. Takahashi, "Performance of wave power generating system installed in breakwater at Sakata port in Japan," in *14th International Offshore Polar Engineering Conference*, Toulon, France,.2004, pp. 202-209

[2] F. Arena, A. Romolo, G. Malara, and A. Ascanelli, "On design and building of a UOWC wave energy converter in the Mediterranean Sea: A Case Study," in *32nd International Conference on Ocean, Offshore and Arctic Engineering*, 2013,

[3] Y. Torre-Enciso, I. Ortubia, L. De Aguileta, and J. Marqués, "Mutriku wave power plant: From the thinking out to the reality," in *8th European Wave Tidal Energy Conference*, Uppsala, Sweden, 1997.

[4] A. F. O. Falcão, and J. C. C. Henriques, "Oscillating-water-column wave energy converters and air turbines: A review,". *Renewable Energy*, 85: 1391–1424, 2016. DOI: 10.1016/j.renene.2015.07.086.

[5] D. V. Evans, "The Oscillating Water Column Wave-energy Device." *IMA Journal of Applied Mathematics*,vol. 22, no. 4, pp. 423-433, 1978.

[6] O. Malmo, and A. Reitan, "Wave-power absorption by an oscillating water column in a channel," *Journal of Fluid Mechanics*, vol. 158: pp. 153-175, 1985. DOI: 10.1017/S0022112085002592.

[7] Z. Deng, Z. Huang, and A. W. K. Law, "Wave power extraction from a bottom-mounted oscillating water column converter with a V-shaped channel," *The Royal Society A Mathematical Physical and Engineering Sciences*, vol. 470,pp. 2167, 2014, DOI: 0.1098/rspa.2014.0074.

[8] D. C. Hong, S. Y. Hong, and S. W. Hong, "Numerical study on the reverse drift force of floating BBDB wave energy absorbers," *Ocean Engineering*, vol. 31, no. 10, pp 1257-1294, 2004, DOI: https://doi.org/10.1016/j.oceaneng.2003.12.007.

[9] Y. Luo, J. R. Nader, P. Cooper, and S. P. Zhu,. "Nonlinear 2D analysis of the efficiency of fixed Oscillating Water Column wave energy converters," *Renewable Energy*, vol. 64, pp. 255-265, 2014, DOI: https://doi.org/10.1016/j.renene.2013.11.007.

[10] T. Vyzikas, S. Deshoulières, O. Giroux, M. Barton, and D. Greaves, "Numerical study of fixed Oscillating Water Column with RANS-type two-phase CFD model," *Renewable Energy*, vol. 102(B), pp. 294-305, 2017, DOI: https://doi.org/10.1016/j.renene.2016.10.044.

[11] A. J. N. A. Sarmento, "Wave flume experiments on two-dimensional oscillating water column wave energy devices," *Experiments in Fluids*, vol. 12, pp, 286-292, 1992, DOI:. https://doi.org/10.1007/BF00187307.

[12] F.He, Z. Huang, and W.K.A. Law, "An experimental study of a floating breakwater with asymmetric pneumatic chambers for wave energy extraction," *Applied Energy*, vol. 106, pp. 222-231, 2013, DOI: 0.1016/j.apenergy.2013.01.013.

[13] R. Q. Wang, D. Z. Ning, C. W. Zhang, Q. P. Zou, and Z. Liu,. "Nonlinear and viscous effects on the hydrodynamic performance of a fixed OWC wave energy converter," *Coastal Engineering*, vol. 131, pp. 42-50, 2018, DOI: 10.1016/j.coastaleng.2017.10.012.

[14] K. Rezanejad, J. Bhattacharjee, and C. G. Soares, "Stepped sea bottom effects on the efficiency of nearshore oscillating water column device," *Ocean Engineering*, vol. 70, pp. 25-38, 2013, DOI: 10.1016/j.oceaneng.2013.05.029.

[15] B. Bouali, and S. Larbi,. "Contribution to the Geometry Optimization of an Oscillating Water Column Wave Energy Converter," *Energy Procedia*, vol. 36, pp. 565 – 573, 2013, DOI: 10.1016/j.egypro.2013.07.065.

[16] J. S. Kim, B. W. Nam, K. H. Kim, S. Park, S. H. Shin, and K. Hong, "A Numerical Study on Hydrodynamic Performance of an Inclined OWC Wave Energy Converter with Nonlinear Turbine-Chamber Interaction based on 3D Potential Flow," *Journal of Marine Science and Engineering*, vol. 8, no. 3, pp. 176, 2020, DOI: 10.3390/jmse8030176.

[17] I. López, R. Carballo, D. M. Fouz, and G. Iglesias, "Design Selection and Geometry in OWC Wave Energy Converters for Performance," *Energies*, vol. 14, no. 6, pp. 1707, 2021, DOI: https://doi.org/10.3390/en14061707.

[18] C. P. Tsai, C. H. Ko, and Y. C. Chen, "Investigation on Performance of a Modified Breakwater-Integrated OWC Wave Energy Converter," *Sustainability*, vol. 10,no. 3,pp. 643, 2018, DOI: 10.3390/su10030643.

[19] C. C. Lin, Y. C. Chow, and Y. Y. Huang, "Geometric Optimization of Cylindrical Flaps of Oscillating using Articifial Oscillating Wave Surge Converters Using Artificial Neutral Network Model," in *13th International Conference on Energy Sustainability*, Bellevue, Washington, USA, 2019.

[20] Z. Liu, Y. Wabg, and X. Hua, "Prediction and optimization of oscillating wave surge converter using machine learning techniques," *Energy Conversion and Management,* vol. 210, pp. 112677, 2020, DOI: https://doi.org/10.1016/j.enconman.2020.112677.

[21] A. Elhanafi, G. Macfarlane, A. Fleming, and Z. Leong, "Scaling and air compressibility effects on a three-dimensional offshore stationary OWC wave energy converter," *Applied Energy*, vol. 189, pp. 1-20, 2017, DOI: 10.1016/j.apenergy.2016.11.095.